Journal of Applied Polymer Science

Soluble-Eggshell-Membrane-Protein-Modified Porous Silk Fibroin Scaffolds with Enhanced Cell Adhesion and Proliferation Properties

Mahesh Kumar Sah, Krishna Pramanik
Department of Biotechnology and Medical Engineering, National Institute of Technology, Rourkela – 769 008, India
Correspondence to: K. Pramanik (E-mail: kpr@nitrkl.ac.in)

ABSTRACT: In this study, a porous silk fibroin (SF) scaffold was modified with soluble eggshell membrane protein (SEP) with the aim of improving the cell affinity properties of the scaffold for tissue regeneration. The pore size and porosity of the prepared scaffold were in the ranges 200–300 μm and 85–90%, respectively. The existence of SEP on the scaffold surface and the structural and thermal stability were confirmed by energy-dispersive X-ray spectroscopy, X-ray diffraction, Fourier transform infrared spectroscopy, differential scanning calorimetry, and thermogravimetric analysis. The cell culture study indicated a significant improvement in the cell adhesion and proliferation of mesenchymal stem cells (MSCs) on the SF scaffold modified with SEP. The cytocompatibility of the SEP-conjugated SF scaffold was confirmed by a 3-(4,5-dimethyltriazol-2-y1)-2,5-diphenyl tetrazolium assay. Thus, this study demonstrated that the biomimic properties of the scaffold could be enhanced by surface modification with SEP. © 2013 Wiley Periodicals, Inc. J. Appl. Polym. Sci. **2014**, *131*, 40138.

KEYWORDS: biocompatibility; bioengineering; biomaterials; porous materials; properties and characterization

Received 14 June 2013; accepted 28 October 2013
DOI: 10.1002/app.40138

INTRODUCTION

Tissue engineering progress in the regeneration of tissues for the restoration, replacement, or improvement of the function of bodily organs needs to include the development of complex, three-dimensional (3D) tissue composite systems that mimic the morphology, architecture, and microenvironments of the target tissues.[1–4] Scaffolds as artificial extracellular matrices for tissue engineering applications must provide a substratum for cell adherence, a structural framework for tissue formation, and integration with the host tissue in addition to acting as a delivery vehicle for bioactive molecules during tissue formation. Thus, ideal biomaterials with desired physicochemical and biological features are essential for tissue engineering. 3D structures with interconnected pores and channels provide a microenvironment for the adherence and proliferation of cells and facilitate the transport of nutrients and metabolic wastes[5] and thus function as an extracellular matrix that plays vital role in determining the fate of cells in tissue regeneration.[6–9] In recent years, a number of natural and synthetic biomaterials have been developed to design scaffolds.[10–15] Because of their excellent biocompatibility and biodegradability, natural biomaterials, such as collagen, silk fibroin (SF), and chitosan, have drawn much attention in the fields of tissue engineering and other biomedical applications.[16–18]

SF derived from the domestic silkworm, *Bombyx mori*, has long been used in medicine in sutures and artificial ligaments. Recently, it has been considered as a biocompatible and mechanically robust biomaterial for bone, cartilage, and ligament tissue engineering.[6,19–25] SFs in the form of hydrogels, nonwoven nets, nonwoven nanofibers, and sponges have been fabricated by various techniques, including freeze gelation, partial dissolution, electrospinning, freeze drying, and salt leaching.[26–30] The challenge still lies in the development of a complex 3D structure of SF with improved scaffold properties to achieve better cell growth, tissue regeneration, and vascularization. Cell–material interaction and, thus, cell adherence and cell proliferation have been reported to directly affect the surface properties of scaffolds.[31,32] It has further been reported that the limited availability of functional groups in SF chains to conjugate specific cell-recognizable signal molecules has restricted their scope in tissue engineering applications.[33] In this context, a number of surface engineering methods that involve the use of a variety of bioactive molecules (e.g., arginyl–glycyl–aspartic acid and other short repetitive peptide chains) have been used to improve certain desired properties of scaffold materials.[33–35] In this study, we used a soluble form of eggshell membrane protein (SEP) as a bioactive molecule for improving the surface properties of SF scaffolds. To the best of our knowledge, this is

Additional Supporting Information may be found in the online version of this article.

the first report on the modification of the surface of porous SF scaffolds with SEP. The reason behind the selection of the eggshell membrane (ESM) biopolymer was the long history of SEP used in Chinese medicine as listed in the Bencao Gangmu as being prescribed for injuries. The ESM is a double-layered, insoluble, and semipermeable sheet located between the eggshell and the egg white;[36] it functionally behaves as a scaffold for biomineralization during to the development of the eggshell and the chick embyo.[37–39] The ESM consists of 70% organic material, 10% inorganic material, and 20% water. The major organic components include insoluble proteins, such as collagens (types I, V, and X), osteopontin, and sialoprotein,[40] with a small amount of carbohydrates and lipids.[41,42] The ESM also has antibacterial and antimicrobial properties and restricts bacterial invasion;[43] thereby, it protects the embryo during development.[44] Maeda and Sasaki[45] reported the use of the ESM as a biological dressing, which showed positive results for burns, and they stated that it had the functional equivalency with the human amniotic membrane.[45] In another study, it was demonstrated that the ESM possessed adherence properties for stromal cells.[46] Because of these properties, ESMs can be used as bioactivity enhancers for scaffolds for tissue regeneration. In recent years, the development of modified biomimetic surfaces have been stressed to support tissue-specific cellular functions, including adhesion, proliferation, differentiation, motility, and gene expression.[47] However, it has been demonstrated that raw ESM can be used for the improvement of tissue-specific cellular function; its shape, size, sheath thickness, and microstructure are not easily controllable, and this limits its applications. Therefore, the SEP, which can be formed into various structures, is highly enviable. The main cause of the insolubility of ESM in water and organic solvents is the presence of a large number of disulfide bond crosslinks[48] between cystine, hydroxylysinonorleicine, and desmosines.[49,50] In 2003, Yi et al.[51] reported the preparation of SEP as a natural bioactive material from natural hen ESM by reductive cleavage with aqueous 3-mercaptopropionic acid in the presence of acetic acid.[52] They also demonstrated that the cell adhesion and proliferation on SEP were comparable to that of cells cultured on collagen type I.[52]

Previous studies have developed SF scaffolds with either defined small pore sizes with limited interconnections[53] or with large pore sizes (>500 μm) with well-connected pores; this limits the tissue engineering applications of SF.[5] Therefore, an attempt has been made in this study to fabricate 3D SF scaffolds with improved surfaces with SEP as a bioactive molecule. The SEP–SF conjugated scaffolds were evaluated to check the improvements in their physical and biochemical characteristics in terms of biodegradability, thermal stability, cell adhesion, and proliferation properties. Thus, we expected to obtain a novel scaffold with improved bioactivity for potential use in tissue engineering.

EXPERIMENTAL

Preparation of the SF Aqueous Solution

Domesticated *B. mori* Silk cocoons were purchased from mulberry farms in the Chittoor district, Hyderabad, India. Fibroin from native silk was extracted by a method mentioned in a previous work.[53] In brief, dried *B. mori* silk cocoon shells were cut into small pieces and degummed in 0.02*M* aqueous sodium carbonate solution for 20 min with stirring. The degummed silks were dissolved in a 9.3*M* LiBr aqueous solution at 70°C for 2.5 h with stirring. The fibroin solution was dialyzed in a cellulose-membrane-based dialysis cassette against deionized water for 3 days with water changes every 6 h and centrifuged at 5–10°C and 9000 rpm for 20 min for storage at 4°C. The concentration of the fibroin solution was measured as 12% w/v. The SF solution was further diluted to 4–6% w/v with water.

Fabrication of the SF Scaffold

Porous scaffolds were prepared from the SF solution by a salt leaching method with NaCl as the porogen. The SF was dissolved at either 10 or 7.5% w/v in 20% v/v formic acid and poured into a circular mold either before or after the NaCl was added. The samples were then left covered in the mold for 24 h and placed in methanol for 30 min. The samples were then subjected to salt leaching in deionized water for 48 h. The salt-leached samples were dried in a vacuum dryer for 24 h at 40°C and stored in a desiccator.[5]

Preparation of SEP

Freshly broken, double-membrane-bound eggshells collected from the canteen of our institute were immediately stored in chilled water. The raw eggshell was washed properly and then peeled off manually from the membrane and kept in aqueous acetic acid (70%) for 2 days to dissolve residual eggshell. This was followed by rinsing with Milli-Q water to remove acidity and drying in a hot-air oven at 50°C for 48 h.[38] Finally, the SEP was obtained by the reductive cleavage of the disulfide bonds present in the ESM by the addition of aqueous 3-mercaptopropionic acid at 90°C in the presence of 10% acetic acid according to a method published earlier.[51,52]

Preparation of the SEP-Conjugated SF Scaffolds

The SF scaffolds were steam-sterilized and dried in ethanol under ambient conditions. The dried scaffolds were soaked in a 2% w/v SEP solution and incubated in a hot-air oven at 37°C for 24 h. The dried samples were crosslinked by the addition of a few drops of a mixture of 1-ethyl-3-[3-(dimethylamino)-propyl] carbodiimide solution (10 mg/mL) mixed with *N*-hydroxysuccinimide solution (10 mg/mL), and they were incubated at 37°C for 12 h.[54,55] The crosslinked samples were desalted and dehydrated with 70 and 99.5% ethanol, respectively. The scaffolds were then dried under an air stream at 37°C for 24 h and kept in a desiccator for further study.

Scanning Electron Microscopy (SEM)

The surface morphology of the silk scaffolds, raw ESM, and SEP-conjugated silk scaffolds were examined by SEM (JEOL JSM-6480LV SEM instrument) at different magnifications. The scaffolds were air-dried, whereas ESM was kept in a 2.8% glutaraldehyde solution overnight. The samples were affixed via carbon tape to the SEM sample holders and vacuum-coated with a 20-nm layer of platinum. SEM was performed at 15 kV and room temperature. The average pore size was calculated with image analysis software (JEOL SMile View). The elemental

composition of SEP was determined by energy-dispersive X-ray spectroscopy analysis.

X-Ray Diffraction (XRD)

The diffraction patterns of the degummed silk fiber, ESM, SF, and SF–SEP scaffold samples were recorded by an X-ray diffractometer (Phillips PW-1830) with Ni-filtered Cu Kα radiation and operating at 35 kV and 30 mA. The samples were scanned from 20 to 70° (2θ) at a scanning rate of 3.0 min^{-1}.

Fourier Transform Infrared (FTIR) Spectroscopy

The FTIR spectra of the scaffolds were obtained with an FTIR spectrometer (model IRPrestige-21, Shimadzu) interfaced with an IR microscope operated in absorbance mode. The spectra were measured and recorded in the 500–4000-cm^{-1} region with a resolution of 4.0 cm^{-1}. The spectra were smoothened with a constant smoothing factor for comparison.

Porosity

The porosity of the scaffolds (π) was measured by a liquid displacement method with hexane as the displacement liquid.[5] A sample of weight was immersed in a known volume (V_1) of hexane in a graduated cylinder. The sample was left covered for 5 min. During this time, the contents in the cylinder underwent an evacuation–repressurization cycle to force the hexane to pass through the pores. The total volume of the hexane and hexane-impregnated scaffold was V_2. The hexane-impregnated scaffold was removed from the cylinder, and the residual hexane volume was recorded as V_3.

π was calculated as follows:

$$\pi = \frac{(V_1 - V_3)}{(V_2 - V_3)}$$

Thermal Properties

The thermal behaviors of the degummed silk, ESM, SF, and SEP–SF scaffolds were analyzed by differential scanning calorimetry (DSC; Mettler Toledo DSC822e) and thermogravimetric analysis (TGA; DTG-6H, Shimadzu). An amount of 10–15 mg of each sample was scanned between in the range 30–300°C at 20°C/min under an N_2 atmosphere for DSC measurement. The TGA measurements were carried out for 1-mg samples at a heating rate of 10°C/min in flowing N_2 heated up to 500°C.

Mechanical Properties

The compressive strength of the scaffolds was determined with a universal testing machine (H10 KS Tinius Olsen) with a 1-kN load cell at room temperature. The dimensions of the SF and SEP-SF scaffolds ($n = 4$) were (11.94 ± 0.22 mm) × (5.64 ± 0.26 mm) and (11.63 ± 0.41 mm) × (5.37 ± 0.63 mm), respectively. The crosshead speed was set at 2 mm/min.

Swelling Behavior and Biodegradability

The swelling behavior and biodegradability of the scaffolds were assayed with a protein-free acellular simulated body fluid medium at pH 7.40 and with an ionic composition of Na^+ (142.0 m*M*), K^+ (5.0 m*M*), Ca^{2+} (2.5 m*M*), Mg^{2+} (1.5 m*M*), Cl^- (147.8 m*M*), HCO_3^- (4.2 m*M*), HPO_4^{2-} (1.0 m*M*), and SO_4^{2-} (0.5 m*M*).[56] The scaffolds were cut into 5.0 × 5.0 mm^2 square pieces with an initial weight (W_0) and were soaked in simulated body fluid at 37°C and pH 7.4 for different time intervals in the range from 30 min to 192 h. The spent medium was discarded, and the excess water on the surface was removed with lint-free tissue paper. The weights of the samples were measured as W_1 (wet) and W_2 (dry). Each experiment was performed in triplicate. The swelling index (S) and biodegradability (B) of the scaffolds were calculated by the following equations:

$$S = \frac{W_1 - W_0}{W_0} \times 100$$

$$B = \frac{W_2 - W_0}{W_0} \times 100$$

Cell Study

Culture of human mesenchymal stem cells (hMSCs). Human umbilical cord blood (UCB) was collected from the nearby Ispat General Hospital, Rourkela, India, from a 37-year-old delivery patient with informed consent and with the approval of the Institutional Ethics Committee. Mononuclear cells were isolated from the UCB by the Ficol gradient centrifugation technique and cultured in Dulbecco's modified Eagle's medium supplemented with 10% fetal calf serum, 1% nonessential amino acids, L-ascorbic acid (0.150 g/L), 1% of 200 m*M* L-glutamine, and 2% of 1*M* HEPES (4-(2-hydroxyethyl)-piperazineethanesulfonic acid), penicillin (100 U/mL) and streptomycin (0.1 mg/mL) at 37°C under 5% CO_2 and 80% relative humidity with the medium being replaced every 2–3 days. When culture flasks became semiconfluent after about 7 days, the cells were trypsinized and serially subcultured. hMSCs harvested with three to four cycles of passage were used for seeding onto the scaffolds.

Cell Seeding and Culture. The scaffolds were neutralized with 10% NH_4OH, washed thoroughly with distilled water, and sterilized by exposure to saturated steam (autoclave) and 75% ethanol for 24 h. This was followed by washing with sterile phosphate-buffered saline (PBS) and drying. The scaffolds were further sterilized by UV radiation. The scaffolds were then placed into a six-well plate. MSCs were seeded with 1 × 10^5 cells/mL into the scaffold and cultured under a standard static state in a CO_2 incubator at 37°C with 5% CO_2 and 80% relative humidity. The cultural medium was replaced every 2–3 days. The MSC-seeded scaffolds were grown *in vitro*. The MSC-seeded scaffold was then assessed for cell attachment, proliferation, and viability at various time points over the 14-day culture period.

Cell Morphology. Photomicrographs of the cells were observed under a phase-contrast microscope (Carl Zeiss, Axiovert 40 C) equipped with a charge coupling device camera. The surface morphology of the MSCs on the scaffolds was examined by SEM (JEOL JSM-6480LV SEM instrument) observation at different magnifications. The adhered hMSCs in the culture plate and cell-seeded scaffolds were kept in a 2.8% glutaraldehyde solution overnight before SEM analysis. The samples were affixed via carbon tape to the SEM sample holders and vacuum-coated with a 20-nm layer of platinum. SEM was performed at a voltage of 15 kV at room temperature.

Cell Counting and Viability. The cell viability study was performed by a 3-(4,5-dimethyltriazol-2-y1)-2,5-diphenyl tetrazolium (MTT) assay according to a procedure reported in the literature.[57,58] In brief, 5 × 10^4 cells were seeded on the scaffolds in a 96-well plate. The cells were incubated at 37°C in a

Table I. Pore Sizes and Porosities of the SF and SEP–SF Scaffolds Prepared with 4–6% w/v regenerated silk fibroin (RSF) with NaCl as a Porogen ($n = 3$)

Sample	NaCl particle size (μm)	Pore size (μm)	Porosity (%)	Remarks
SF	<100	30–70	85–88	Not interconnected
SF	100–200	90–150	81–86	Interconnected and suitable for skin TE[62]
SF	200–300	140–230	87–89	Interconnected but moderately applicable for osteogenesis[63]
SF	300–500	225–350	90–93	Interconnected and more applicable for osteogenesis and chondrogenesis[63,64]
SEP–SF	300–500	200–300	85–90	Interconnected and more applicable for osteogenesis and chondrogenesis[63,64]

humidified atmosphere with 5% CO_2. After 24 h of incubation, the supernatant of each well was replaced with MTT diluted in serum-free medium, and the plates were incubated at 37°C for 4 h. A 10% sodium dodecyl sulfate/0.04*N* HCl solution was then added to the supernatant, and the plates were reincubated for 24 h. A volume of 200 μL of solution was transferred to a clean 96-well plate, and the optical density was measured at 595 nm with an ASYS EXPERT PLUS spectrometric microplate reader.

Alkaline Phosphatase (ALP) Assay. The ALP activity of the UCB-derived hMSCs grown on the developed scaffold samples was measured to assess the osteogenic differentiation in a time course. After day 1, the medium was changed to osteogenic differentiation medium, and samples were removed on days 7 and 14 for the measurement of ALP activity. The scaffolds were thoroughly washed three times with PBS to remove the residual serum, and then, 1 mL of 0.02% Triton X-100 was placed on the scaffold to dissolve the cells. This was followed by transfer into a 1.5-mL tube for sonication. The solutions were centrifuged at 14,000 rpm at 4°C for 15 min, and the supernatant was transferred to fresh 1.5-mL tubes. Volumes of 100 μL of 1 mol/L trishydroxymethylaminomethane HCl, 20 μL of 5 mmol/L $MgCl_2$, and 20 μL of 5 mmol/L *p*-nitrophenyl phosphate were added to the supernatant, and it was incubated for 30 min at 37°C. The reaction was stopped with 50 μL of stop solution (1*N* NaOH), and the absorbance was read at 410 nm. *p*-Nitrophenol with known concentrations was used to prepare the standard curve.[59] All solutions were components of the ALP assay kit (Abcam, Cambridge, MA, ab83369-500).

***In Vivo* Transplantation for Biocompatibility.** Transplantation of the scaffolds under the skin of 4- to 6-week-old imprinting control region (ICR) recipient mice was performed as described previously[60] with modification. Briefly, the mice were anesthetized with an intraperitoneal injection of Avertin (tribromoethanol, 0.25 mg/g of body weight; 2-methyl-2-butanol, 0.16 mL/g), and the skin was prepared and sterilized by 70% v/v ethanol. An approximately 1-cm linear incision was made on the dorsolateral side of the skin, and a small pouch was created in the subcutaneous layer. The scaffold (5×5 mm^2), one per mouse, was transplanted into the surgically created subcutaneous pouch, and the incision was closed with a nylon suture. All animals were monitored routinely for skin and systemic diseases, if any. One month after the transplantation, the recipients were sacrificed by cervical dislocation, and the samples were explanted. In addition, the skin around the site of transplantation was excised for histological analysis. The excised skin also included part of the apparently normal skin around the site of transplantation. The skin samples were fixed in 10% v/v neutral buffered formalin and dehydrated in ascending grades (40, 60, 80, 95, and 100% ethanol and embedded in paraffin wax. The specimens were sectioned into 5 μm thick slices by a microtome and were examined histologically after hematoxylin and eosin staining. All of the experiments were performed under aseptic conditions in compliance with the *Guide for the Care and Use of Animals in Research and Teaching*, published by the Federation of Animal Science Societies (3rd ed., 2000), and were approved by the Institutional Biosafety and Ethical Committee. All efforts were made to ameliorate the suffering of the animals.

Statistical Analysis

For analysis, all data were expressed as the average plus or minus standard deviation for a number of three replicates. Statistical significance was determined for all of the groups, and *p* values were generated by analysis of variance with the Dunnett test for multiple comparisons to one control ($p < 0.05$, $n \geq 3$ assays). This method relies on assumptions of normality and homogeneity of the variances of the distributions.

RESULTS AND DISCUSSION

Pore Size and π

SF scaffolds with various pore sizes and πs were prepared with NaCl as a porogen and 4–6% SF solution.[35] Table I shows the pore sizes and πs of the scaffolds prepared in this study. The pore size was measured from the SEM images shown in Figure 1. The particle size of the porogen was shown to have a great influence on the pore size and π. Scaffolds with pore sizes in the range 30–350 μm were obtained with a porogen of with sizes of less than 100 μm [Figure 1(a)], 100–200 μm [Figure 1(b)], 200–300 μm [Figure 1(c)], and 300–500 μm [Figure 1(d)]. The πs and pore sizes of the scaffolds obtained were in the ranges 81–93% and 30–350 μm, respectively, with a porogen in the size range 100–500 μm. A particle size below 100 μm or above 500 μm (data not shown) was not favorable for the scaffold because of the limitation in pore interconnectivity.[62] The pore size of the scaffolds was 80–90% smaller than the particle size of NaCl used in the process; this reflected the partial dissolution of the crystal surface. In aqueous-derived SF, scaffolds

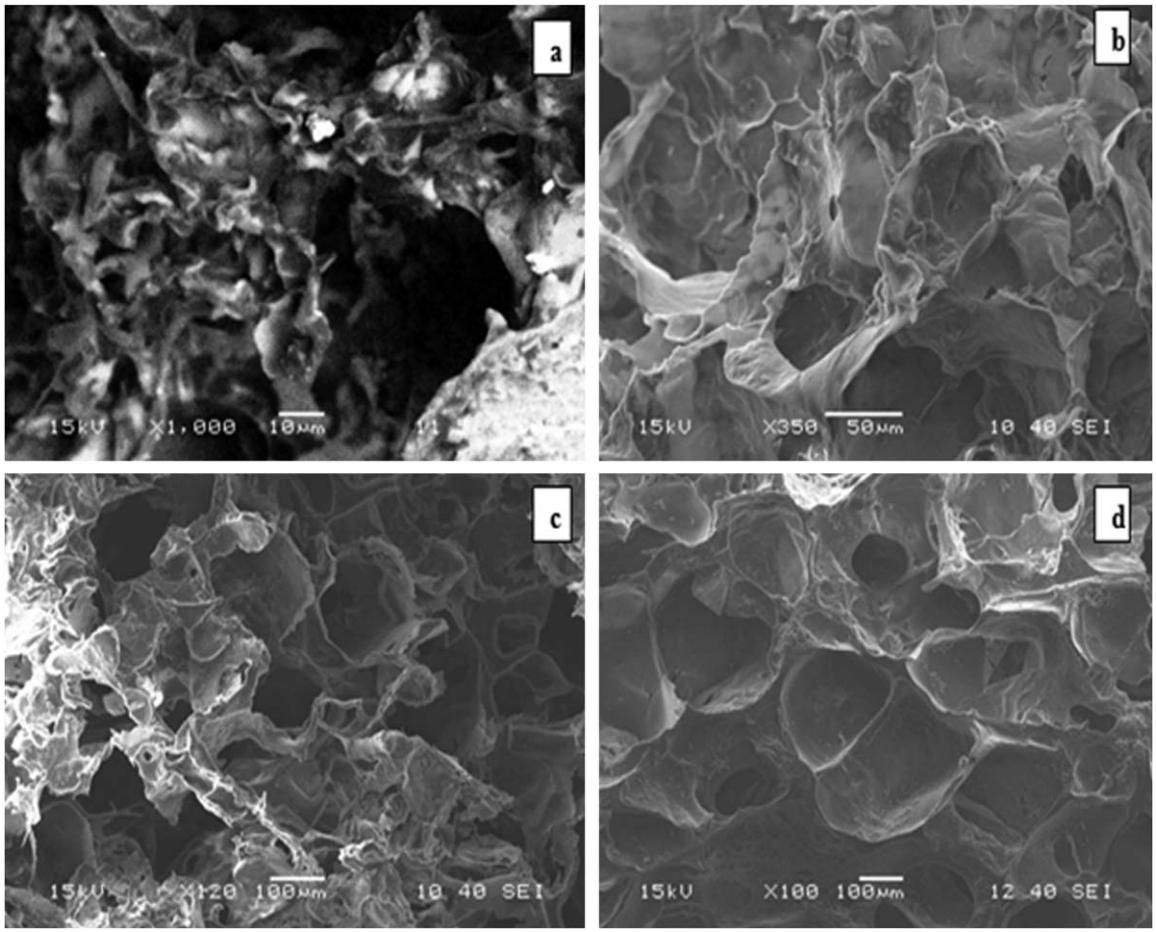

Figure 1. SEM of the SF scaffolds prepared by the salt-leaching method with NaCl as a porogen: (a) less than 100, (b) 100–200, (c) 200–300, and (d) 300–500 μm.

prepared with the particle size of NaCl resulted in a similar trend in pore size. The recommended pore size for a scaffold system based on the cell size and migration was a minimum of 100 μm, as reported by Hulbert et al.[62] However, subsequent studies have shown better vascularization and cell migration in implants with pore sizes greater than 300 μm.[63,65,66]

SEP-Conjugated SF Scaffolds

SF scaffolds with pore sizes of 225–350 μm were further modified with SEP as a bioactive material. As a chemical crosslinker, EDC reacted with the carboxylic acid groups of the peptide chain, which could then bind to the amino group in the reaction mixture of SEP loaded in the SF scaffold.[67] The SEM image (Figure 2) showed the porous structure of the SEP–SF scaffold. We observed that the pore size and π were not affected much by the conjugation with 2% w/v SEP. The pore size of the modified scaffold was found to be in the range 200–300 μm with a porosity of approximately 85–90%. The slight reduction in the porosity and pore size may have been due to a blockage of the pores after SEP conjugation.

Elemental Analysis

Elemental analysis was done to measure the finite elements of the SF, SEP, and SEP–SF scaffolds. Each analysis was performed in triplicate, and the average value is shown in Table II. The elemental composition of SF and SEP were very close to the experimental data published by Wang et al.[68] and Yi et al.[52] The composition of SEP–SF indicated the immobilization of the SEP throughout the SF scaffold.

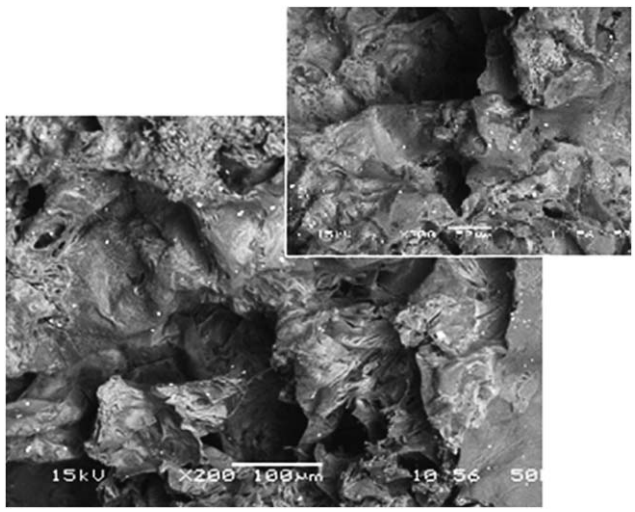

Figure 2. SEM of the SEP-conjugated SF scaffold.

Table II. Elemental Compositions of the SEP, SF, and SEP–SF Scaffolds

Sample	Weight (mg)	C (wt %)	H (wt %)	N (wt %)	O (wt %)	S (wt %)
SF	2.001	43.30	6.04	14.78	27.9	0.35
SEP	1.989	46.53	6.7	15.93	11.76	2.89
SEP-SF	2.015	45.33	6.51	15.11	22.7	0.93

Structural Analysis of the Scaffolds

The XRD patterns of the SEP and SF scaffolds are depicted in Figure 3. According to research on the molecular conformation of the SF protein,[69] the XRD pattern of the SF scaffold [Figure 3(a)] was determined as 12.5° (2θ) for the α-helix structure (silk I) and 20.4° (2θ) for the β-sheet structure (silk II). The XRD curve of the SEP–SF scaffold [Figure 3(b)] showed two peaks around 12.6° (2θ) and 20.5° (2θ); these indicated the coexistence of an α helix and β sheet with partial induction of the α helix to the β sheet due to SEP conjugation. The XRD pattern of SEP [Figure 3(c)] showed a broad peak at 20.2° (2θ), which indicated the amorphous nature of the material.

The functional properties of the scaffolds were studied by FTIR spectroscopy. As shown in Figure 4, the amide I band (1600–1700 cm^{-1}) was associated with the stretching vibrations of the carbonyl groups (C═O bond) along the polypeptide backbone[70] and was found to be most important for the protein's secondary structure.[71] The FTIR spectra of the SF scaffold showed strong absorption bands for amide I (1654 cm^{-1}), amide II (1519 cm^{-1}), amide III (1220 cm^{-1}), and amide V (555 cm^{-1}); these could be attributed mainly to random coil conformation and the helix. It was indicated that the formation of the SF scaffolds from regenerated SF solutions induced a conformational transition from random coil to α helix. The FTIR spectrum of SEP showed the absorption bands of amide A (3215 cm^{-1}), amide B (2126 cm^{-1}), amide I (1654 cm^{-1}), amide II (1545 cm^{-1}), and amide III (1253 cm^{-1}). The amide A and B bands were related

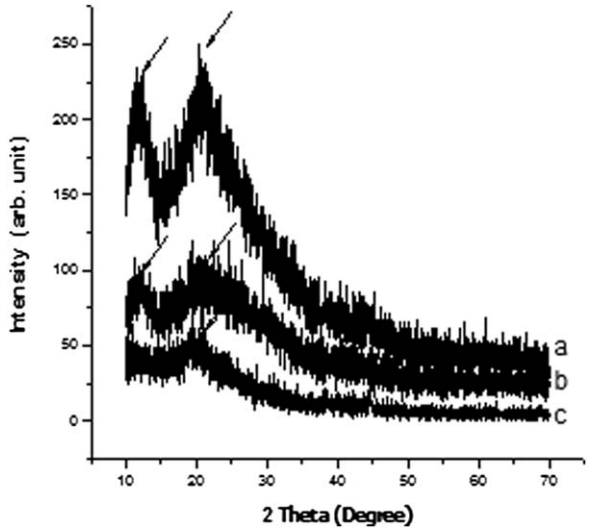

Figure 3. XRD patterns of (a) the SF scaffold, (b) the SEP–SF scaffold, and (c) SEP.

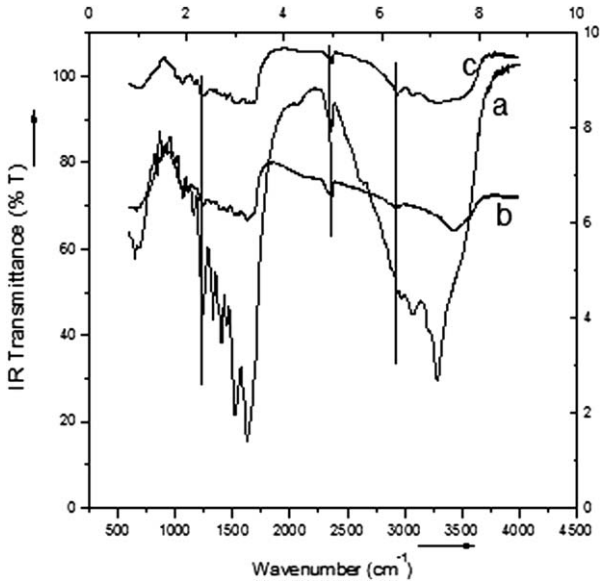

Figure 4. FTIR spectra of (a) the SF scaffold, (b) the SEP–SF scaffold, and (c) SEP.

to NH stretching coupled with H bonding and CH_2 asymmetrical stretching, whereas amide II was associated with NH bending and CN stretching. These results were very close to those of the FTIR spectrum of collagen from yellow fin tuna dorsal skin.[68] Furthermore, both the amide B group (2126 cm^{-1}) of SEP and the characteristic amide groups of SF (amide I at 1654 cm^{-1} and amide II at 1519 cm^{-1})[70] were present in the SEP–SF scaffold; this confirmed the proper conjugation of SEP to SF by covalent immobilization with EDC/*N*-hydroxysuccinimide as a crosslinking agent to link the carboxyl groups of SEP to the primary amines of SF.

Compressive Strength

The stress–strain graphs of the prepared scaffolds are shown in [Figure 5(a,b)]. The SF and SEP–SF scaffolds had different line patterns, which were the typical patterns of elastic/plastic material. For both scaffolds investigated, the steepest portion of the stress–strain curve occurred in the range of 0–4% strain. The uncoated fibroin scaffold broke between 200 and 300 KPa with a strain of 1.8–2.8%. The mechanical resistance was increased after SEP coating and supported breaking forces higher than 3 N and strains over 4%. The average compressive strength for SF was found to be 279.8 ± 36.2 KPa, and that for SEP–SF scaffolds was found to be 321.5 ± 42.2 KPa. The higher compressive strength of SEP compared to that of SF has also been reported earlier.[52] Furthermore, a difference in the stress–strain curve representing different mechanical behaviors of SEP–SF when compared with those of the SF scaffold was observed. This may have been due to the increase in the compressive strength imparted by the conjugation of SEP to SF.

Swelling Behavior and Biodegradability

Water molecules, the component of the coordination bond that act as the swelling agent, were undoubtedly needed for the dissolution of SF. Figures 6 and 7 show the swelling behavior and biodegradability of the scaffolds. The results indicate the

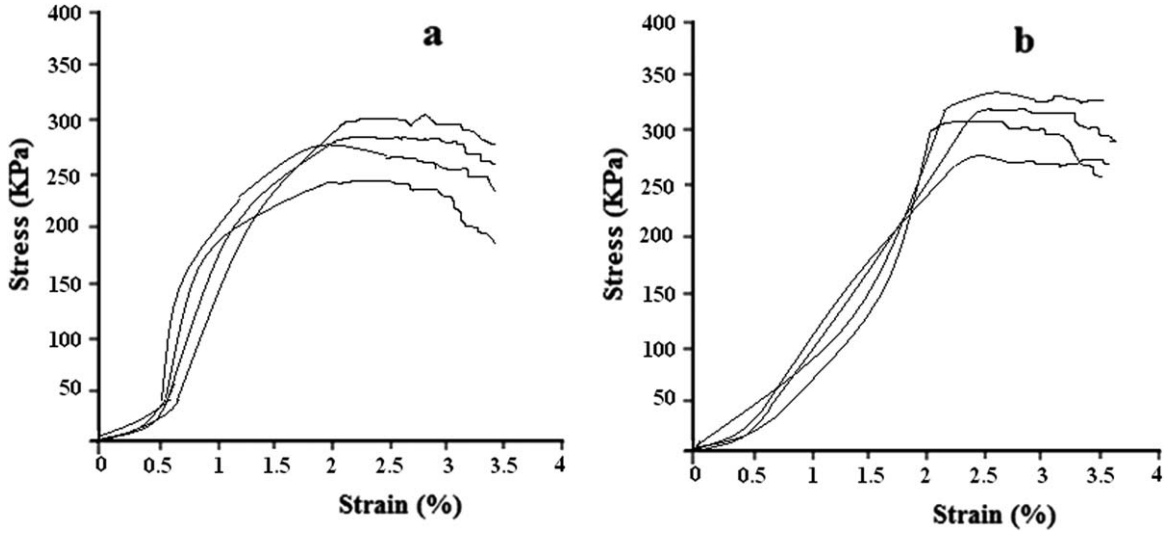

Figure 5. Stress–strain curves of the (a) SF and (b) SEP–SF scaffolds.

swelling of SF scaffold as 60.3% after 30 min; it increased to 133.36% after 48 h. A similar trend was observed with the SF scaffold modified with SEP with a slight increase in *S* during the period of study. The increase in *S* may have been due to the enhanced hydrophilicity of the scaffold surface after SEP conjugation.

Initial weight losses of 0.08 and 0.04% were observed in the SF and SEP–SF scaffolds. However, the maximum weight losses achieved were 1.89 and 2.38% for SF and SF–SEP, respectively, after 192 h. The increase in biodegradation in the conjugated scaffold as compared to the control may have been due to the enhanced hydrophilicity and partial surface erosion from the scaffolds in PBS.

Cell Morphology

The SEM images of the cell–scaffold constructs are shown in Figure 8. After 1 day of cell seeding, the cells started to adhere and aggregate in the pores of both the SF and SEP–SF scaffolds. Although initially cell adherence followed a similar trend for both of the scaffolds, the cell adherence and spreading were found to cover uniformly throughout the SEP–SF scaffolds during the 7 to 14 days of culturing.

Cell Adhesion and Proliferation

Attachment and the proliferation of cells on a given substrate are fundamentals for a functional tissue engineering scaffold. The cell viability was determined on the basis of the linear correlation between the cell count and optical density 570 (OD570) value of MTT formazan.[70] The number of cells were observed to increase with increasing culture period with both the SF and SEP–SF scaffolds, although at various proliferation rates, as shown in Figure 9. The viability of the proliferated cells on the SF scaffolds was found to gradually increase from 0.191 ± 0.018 to 0.493 ± 0.015 during the 14 days of culturing (Figure 9). The proliferation rate was observed to be higher with the SF–SEP scaffold, where it achieved a value of 0.675 ± 0.031 optical density (OD) on day 14. Cells entrapped inside the scaffold without adherence did not show much spreading or proliferation at all and did not survive during

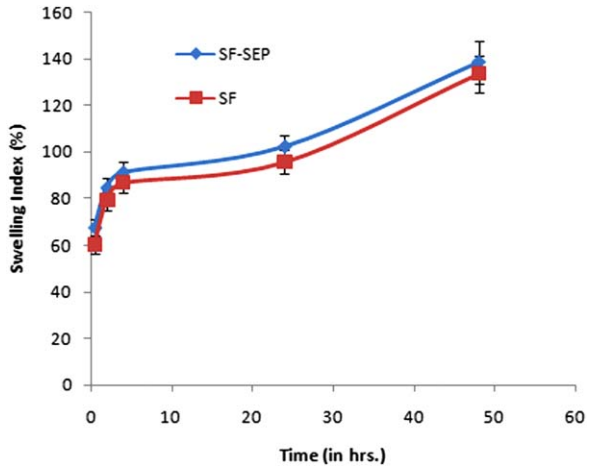

Figure 6. Swelling behavior of the scaffolds. [Color figure can be viewed in the online issue, which is available at wileyonlinelibrary.com.]

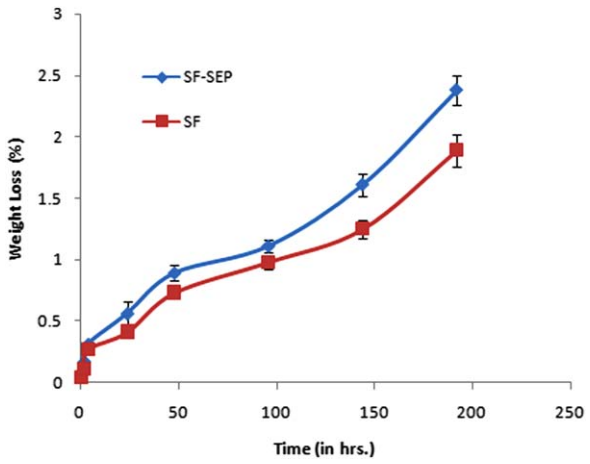

Figure 7. Biodegradability of the salt-leached SF and SEP–SF scaffolds. [Color figure can be viewed in the online issue, which is available at wileyonlinelibrary.com.]

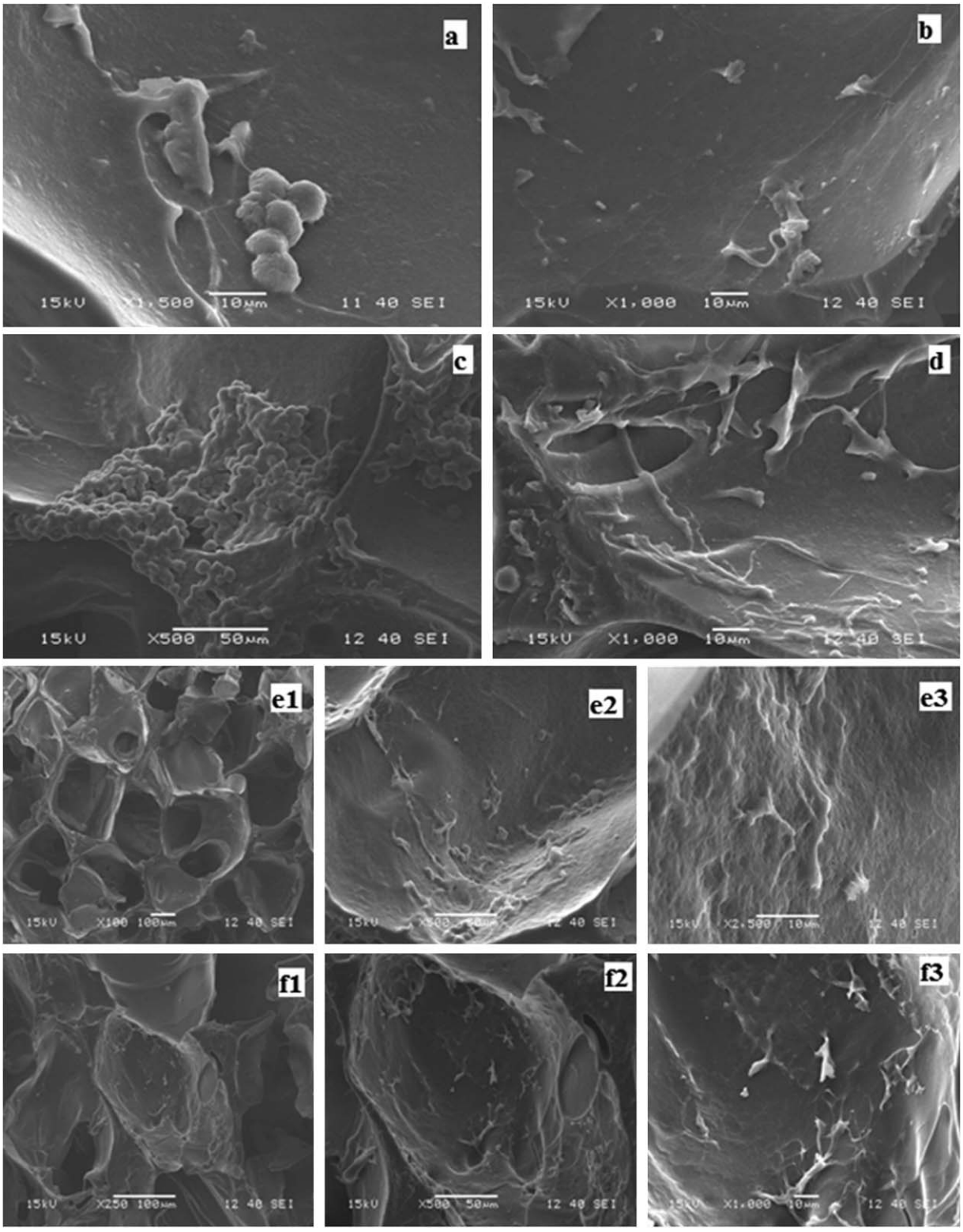

Figure 8. SEM of the cell–scaffold construct on days (a,b) 3, (c,d) 7, and (e,f) 14 of culturing. The figure shows the progressive adherence of the MSCs in (b,d,e) SEP-conjugated scaffolds and (a,c) controls. The SEP-conjugated scaffolds showed early adherence and morphological changes in the cell shape in comparison with the controls. After 14 days of MSC culturing in the (f1–f3) modified scaffolds versus the (e1–e3) control SF scaffolds. The cells were spread all over the scaffolds, as shown in the SEM images. The scale bars represent (a,b,d,e3,f3) 10 and (c,e1,e2,f1,f2) 50 μm.

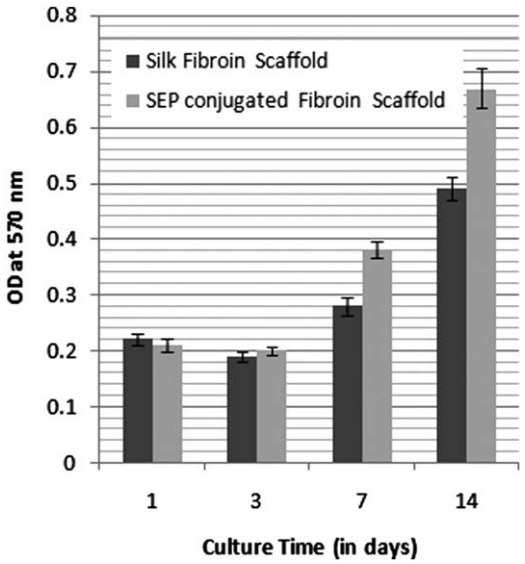

Figure 9. Comparison of the optical density of the MTT formazan on the SF and SEP–SF scaffolds during the 14-day culture periods ($p < 0.05$, $n = 3$).

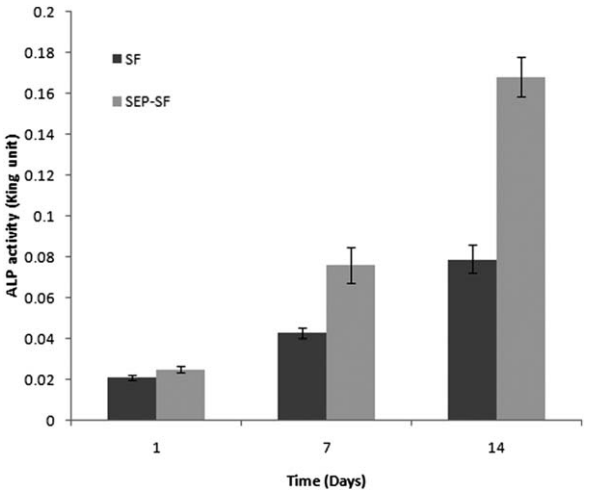

Figure 10. ALP activity assay of the hMSCs grown on the SF and SEP–SF scaffolds for 1, 7, and 14 days. Each value represents the mean value and standard deviation ($p < 0.05$, $n = 3$).

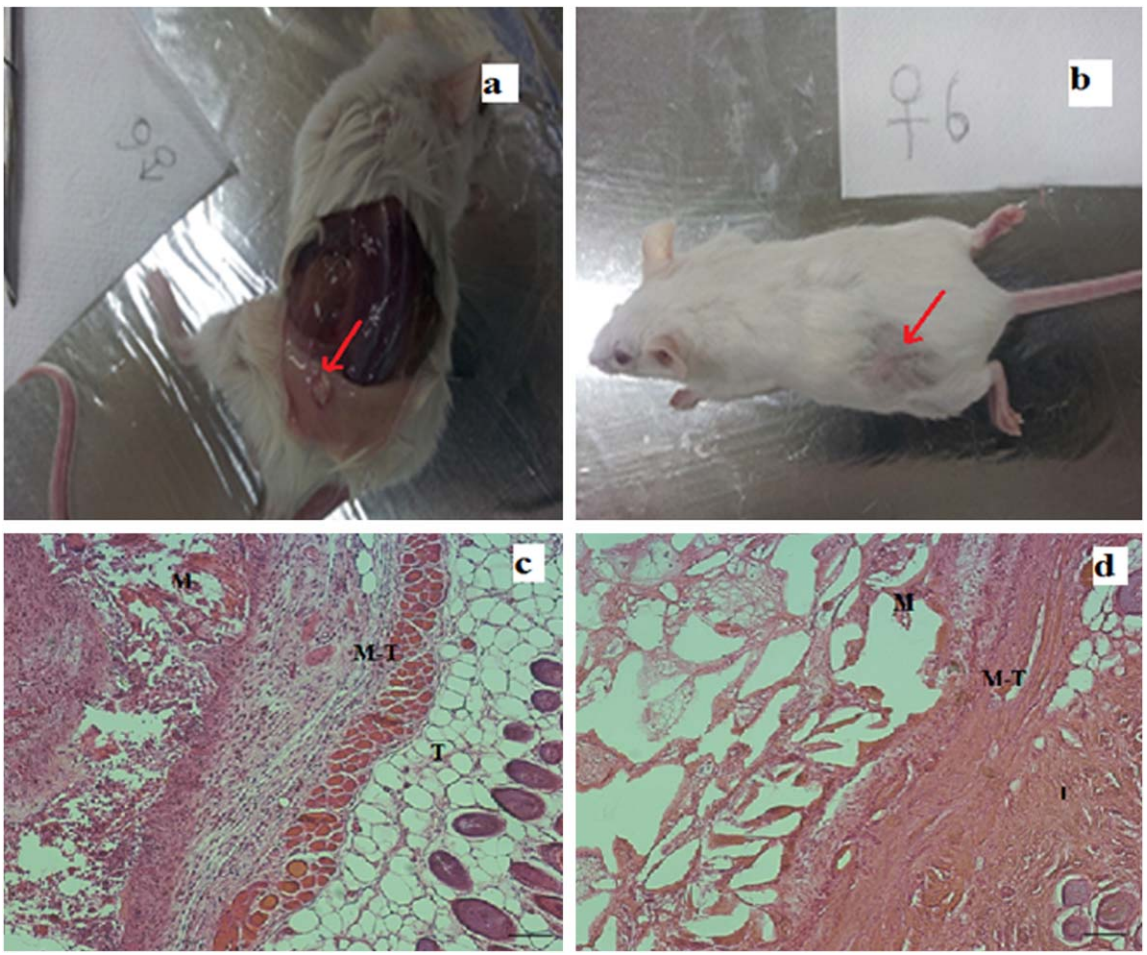

Figure 11. *In vivo* study of the SE–SF scaffolds in the ICR mice strain for the biocompatibility study: (a) implantation of the scaffold in the male and (b) surgical recovery after 1 month in the female. The histological section of the skin and subcutaneous tissue to the SE–SF scaffolds after implantation in the ICR mice model after (c) 7 days and (d) 4 weeks. The bar indicates 200 μm (M, the implanted SEP–SF scaffold; T, the subcutaneous connective tissue; M–T, scaffold–tissue interface). [Color figure can be viewed in the online issue, which is available at wileyonlinelibrary.com.]

further cell culturing, as indicated by the MTT assay on the 3rd day. Cells adhering over the surface and inside the scaffold were found to be growing, proliferating, and differentiating. However, a confluence of a large number of cells was observed on the 7th day of culturing to be entirely covering the conjugated scaffold compared to the SF scaffold. After 14 days of culturing, the cells more prominently spread on the pore surface with a flat morphology [Figure 9(f)]. Thus, it was demonstrated in this study that the modified SF scaffold was more effective than the SF scaffold; this was evident from an improved cell proliferation and cell viability observed with a conjugated scaffold. This enhanced expansion of cell culturing could be attributed mainly to the SEP-mediated improved surface hydrophilicity rather than to the scaffold morphology change because there was no significant change in the morphology due to the 2% SEP solution used in this study.

ALP Activity of the Scaffolds

The osteogenic differentiation of the hMSCs on the SF and SEP-conjugated SF scaffolds was determined by endogenous ALP activity measured on days 1, 7, and 14. Both groups showed enhanced ALP activity over the culture period. However, the SEP-conjugated SF scaffold showed significantly higher activity than the SF scaffold ($p < 0.01$), as shown in Figure 10. This implied that the conjugated scaffolds prepared from SF with SEP were more favorable for cell differentiation.

In Vivo Study of the SEP–SF Scaffolds

Transplantation of the SEP–SF scaffolds was performed under a surgically created subcutaneous pouch in apparently healthy mice [both male and female to determine gender effects, if any; Figure 11(a)]. During the period of the experiment, all mice remained healthy and did not show any wound complications, and no inflammatory and/or adverse tissue reactions were observed. Thus, the transplanted scaffolds did not have any adverse effects on the physiology of the animals [Figure 11(b)]. After 1 and 4 weeks of transplantation, the mice were sacrificed, and the host tissue reaction was analyzed by hematoxylin and eosin (H&E) staining.

After 7 days of implantation, more fibroblasts were grown into the scaffold, and inflammatory cells were in existence [Figure 11(c)]. However, when the test had proceeded for 4 weeks, a large number of fibroblasts had infiltrated into the scaffold, and the morphology of scaffold was close to the surrounding dermal tissue [Figure 11(d)]. Thus, we concluded that the SEP–SF scaffold supported the attachment and proliferation *in vivo* condition without causing infection, inflammation, and/or tissue cell death.

CONCLUSIONS

In this study, novel SEP-modified SF porous scaffolds were fabricated by a salt-leaching technique. Elemental analysis, XRD, FTIR spectroscopy, DSC, and TGA studies indicated the successful conjugation of SEP over the SF scaffold and confirmed the structural and thermal stability of the modified scaffolds. The *in vitro* cell culture study showed significantly higher cell adhesion and proliferation on the conjugated scaffold. The *in vivo* animal model evaluation depicted the biocompatibility of the SEP–SF scaffolds. Therefore, this study demonstrated that the porous SF scaffolds modified with SEP offered enhanced cell adhesion and proliferation and, hence, improved biocompatibility to facilitate its application in practical tissue engineering.

ACKNOWLEDGMENTS

The authors are thankful to the Department of Biotechnology (New Delhi, India) and the Government of India for providing the research facility and the National Institute of Technology (Rourkela, India) for providing a fellowship to one of the authors.

REFERENCES

1. Langer, R.; Vacanti, J. P. *Science* **1993**, *260*, 920.
2. Ma, P. X. *Mater. Today* **2004**, *7*, 30.
3. Ma, P. X. Tissue Engineering Encyclopedia of Polymer Science and Technology, 3rd ed.; Wiley: New York, **2005**; p 261.
4. Rice, M. A.; Dodson, B. T.; Arthur, J. A.; Anseth, K. S. *Otolaryngol. Clin. North Am.* **2005**, *38*, 199.
5. Kim, U. J.; Park, J.; Kim, H. J.; Wada, M.; Kaplan, D. L. *Biomaterials* **2005**, *26*, 2775.
6. Altman, G. H.; Horan, R. L.; Lu, H. H.; Moreau, J.; Martin, I.; Richmond, J. C.; Kaplan, D. L. *Biomaterials* **2002**, *23*, 4131.
7. Freed, L. E.; Vunjaknovakovic, G.; Biron, R. J.; Eagles, D. B.; Lesnoy, D. C.; Barlow, S. K.; Langer, R. *Biotechnology* **1994**, *12*, 689.
8. Mayer, J.; Karamuk, E.; Akaike, T.; Wintermantel, E. *J. Controlled Release* **2000**, *64*, 81.
9. Hutmacher, D. W. *Biomaterials* **2000**, *21*, 2529.
10. Chen, Y. L.; Lee, H. P.; Chan, H. Y.; Sung, L. Y.; Chen, H. C.; Hu, Y. C. *Biomaterials* **2007**, *28*, 2294.
11. Oki, A.; Qiu, X.; Alawode, O.; Foley, B. *Mater. Lett.* **2006**, *60*, 2751.
12. Duan, X.; Sheardown, H. *Biomaterials* **2006**, *27*, 4608.
13. Lu, Q.; Zhang, S.; Hu, K.; Feng, Q.; Cao, C.; Cui, F. *Biomaterials* **2007**, *28*, 2306.
14. Torres, F. G.; Nazhat, S. N.; Sheikh, M. F.; Maquet, V.; Boccaccini, A. R. *Compos. Sci. Technol.* **2007**, *67*, 1139.
15. Wang, Y.; Blasioli, D. J.; Kim, H. J.; Kim, H. S.; Kaplan, D. L. *Biomaterials* **2006**, *27*, 4434.
16. Araki, Y.; Akahoshi, K.; Harada, N.; Chijiiwa, Y.; Sasaki, I.; Nawata, H. *Endoscopy* **2001**, *33*, 85.
17. Gomathi, K.; Gopinath, D.; Ahmed, M. R.; Jayakumar, R. *Biomaterials* **2003**, *24*, 2767.
18. Remy, M.; Valli, N.; Brethes, D.; Labrugere, C.; Porte-Durrieu, M. C.; Dobrova, N. B.; Novikova, S. P.; Gorodkov, A. J.; Bordenave, L. *Biomaterials* **1999**, *20*, 241.
19. Altman, G. H.; Diaz, F.; Jakuba, C.; Calabro, T.; Horan, R. L.; Chen, J.; Lu, H.; Richmond, J.; Kaplan, D. L. *Biomaterials* **2003**, *24*, 401.
20. Cappello, J.; Crissman, J. W.; Crissman, M.; Ferrari, F. A.; Textor, G.; Wallis, O.; Whitledge, J. R.; Zhou, X.; Burman, D.;

Aukerman, L.; Stedronsky, E. R. *J. Controlled Release* **1998**, *53*, 105.

21. Wong, P. F. C.; Kaplan, D. L. *Adv. Drug Delivery Rev.* **2002**, *54*, 1131.
22. Dinerman, A. A.; Cappello, J.; Ghandehari, H.; Hoag, S. W. *J. Controlled Release* **2002**, *82*, 277.
23. Megeed, Z.; Cappello, J.; Ghandehari, H. *Adv. Drug Delivery Rev.* **2002**, *54*, 1075.
24. Petrini, P.; Parolari, C.; Tanzi, M. C. *J. Mater. Sci. Mater. Med.* **2001**, *12*, 849.
25. Panilaitis, B.; Altman, G. H.; Chen, J. S.; Jin, H. J.; Karageorgiou, V.; Kaplan, D. L. *Biomaterials* **2003**, *24*, 3079.
26. Sah, M. K.; Pramanik, K. *Afr. J. Biotechnol.* **2011**, *10*, 7878.
27. Agrawal, C. M.; Ray, R. B. *J. Biomed. Mater. Res.* **2001**, *55*, 141.
28. Liu, L.; Liu, J.; Wang, M.; Min, S.; Cai, Y.; Zhu, L.; Yao, J. *J. Biomater. Sci. Polym. Ed.* **2008**, *19*, 325.
29. Ohgo, K.; Zhao, C.; Kobayashi, M.; Asakura, T. *Polymer* **2003**, *44*, 841.
30. Wang, Y.; Rudym, D. D.; Walsh, A.; Abrahamsen, L.; Kim, H. J.; Kim, H. S.; Kirker-Head, C.; Kaplan, D. L. *Biomaterials* **2008**, *29*, 3415.
31. Dobkowski, J.; Kolkos, R.; Kaminski, J.; Kowalczynska, H. M. *J. Biomed. Mater. Res.* **1999**, *47*, 234.
32. Yaylaoglu, M. B.; Yildiz, C.; Korkusuz, F.; Hasirci, V. *Biomaterials* **1999**, *20*, 1513.
33. Yang, X. B.; Roach, H. I.; Clarke, N. M. P.; Howdle, S. M.; Quirk, R.; Shakesheff, K. M.; Oreffo, R. O. C. *Bone* **2001**, *29*, 523.
34. Mann, B. K.; West, J. L. *J. Biomed. Mater. Res.* **2002**, *60*, 86.
35. Lee, J. H.; Ju, Y. M.; Kim, D. M. *Biomaterials* **2000**, *21*, 683.
36. Carrino, D. D.; Dennis, J. E.; Wu, T. M.; Arias, J. L.; Fernández, M. S.; Rodríguez, J. P.; Fink, D. J.; Heuer, A. H.; Caplan, A. I. *Connect. Tissue Res.* **1996**, *35*, 325.
37. Nakano, T.; Ikawa, N. I.; Ozimek, L. *Poultry Sci.* **2003**, *82*, 510.
38. Tsai, W. T.; Yang, J. M.; Lai, C. W.; Cheng, Y. H.; Lin, C. C.; Yeh, C. W. *Bioresour. Technol.* **2006**, *97*, 488.
39. Rose, M. L.; Hincke, M. T. *Cell Mol. Life Sci.* **2009**, *66*, 2707.
40. Nys, Y.; Gautron, J.; McKee, M. D.; Gautron, J. M.; Hincke, M. T. *World's Poultry Sci. J.* **2001**, *57*, 401.
41. Suyama, K.; Nakamura, H.; Ishida, M.; Adachi, S. *J. Agric. Food Chem.* **1997**, *25*, 799.
42. Baker, J. R.; Balch, D. A. *Biochem. J.* **1962**, *82*, 352.
43. Ahlborn, G.; Sheldon, B. W. *Poultry Sci.* **2005**, *84*, 1935.
44. Burley, R. W.; Vadehra, D. V. The Avian Egg, Chemistry and Biology; Wiley: New York, **1989**; p 472.
45. Maeda, K.; Sasaki, Y. *Burns Incl. Therm. Inj.* **1982**, *8*, 313.
46. Tavassoli, M. *Experientia* **1983**, *39*, 411.
47. von der Mark, K.; Park, J.; Bauer, S.; Schmuki, P. *Cell Tissue Res.* **2010**, *339*, 131.
48. Takahashi, K.; Shirai, K.; Kitamura, M.; Hattori, M. *Biosci. Biotechnol. Biochem.* **1996**, *60*, 1299.
49. Crombie, G.; Snider, R.; Faris, B.; Franxblm, C. *Biochem. Biophys. Acta* **1981**, *640*, 365.
50. Leach, R. M.; Rucker, R. B.; Duke, G. P. *Arch. Biochem. Biophys.* **1981**, *207*, 353.
51. Yi, F.; Yu, J.; Guo, Z. X.; Zhang, L. X.; Li, Q. *Macromol. Biosci.* **2003**, *3*, 234.
52. Yi, F.; Guo, Z. X.; Zhang, L. X.; Yu, J.; Li, Q. *Biomaterials* **2004**, *25*, 4591.
53. Nazarov, R.; Jin, H. J.; Kaplan, D. L. *Biomacromolecules* **2004**, *5*, 718.
54. Hermanson, G. T. Bioconjugate Techniques; Academic: New York, **1996**; p 785.
55. Hafemann, B.; Ghofrani, K.; Gattner, H. G.; Stieve, H.; Pallua, N. *J. Mater. Sci. Mater. Med.* **2001**, *12*, 437.
56. Kim, H. M.; Kishimoto, K.; Miyaji, F.; Kokubo, T.; Yao, T.; Suetsugu, Y.; Tanaka, J.; Nakamura, T. *J. Biomed. Mater. Res.* **1999**, *46*, 228.
57. Cory, A. H.; Owen, T. C.; Barltrop, J. A.; Cory, J. G. *Cancer Commun.* **1991**, *3*, 207.
58. Wilson, A. P. In Animal Cell Culture, 3rd ed.; Masters, J. R. W., Ed.; Oxford University Press: Oxford, **2000**; p 175.
59. Sun, X. J.; Zhang, Z. Y.; Wang, S. Y.; Gittens, S. A.; Jiang, X. Q.; Chou, L. L. *Clin. Oral Implants Res.* **2008**, *19*, 804.
60. Jung, H.; Kwak, B.; Yang, H. S.; Tae, G.; Kim, J.-S.; Shin, K. *Colloids Surf. A* **2008**, *313*, 562.
61. Kodali, V. K.; Gannon, S. A.; Paramasivam, S.; Raje, S.; Polenova, T.; Thorpe, C. *PLoS One* **2011**, 6, e18187.
62. Hulbert, S. F.; Young, F. A.; Mathews, R. S.; Klawitter, J. J.; Talbert, C. D.; Stelling, F. H. *J. Biomed. Mater. Res.* **1970**, *4*, 433.
63. Karageorgiou, V.; Kaplan, D. *Biomaterials* **2005**, *26*, 5474.
64. Yang, J.; Shi, G.; Bei, J.; Wang, S.; Cao, Y.; Shang, Q.; Yang, G.; Wang, W. *J. Biomed. Mater. Res.* **2002**, *62*, 438.
65. Murphy, C. M.; Haugh, M. G.; O'Brien, F. *J. Biomaterials* **2010**, *31*, 461.
66. deGroot, J. H.; de Vrijer, R.; Pennings, A. J.; Klompmaker, J.; Veth, R. P. H.; Jansen, H. W. B. *Biomaterials* **1996**, *17*, 163.
67. Burdick, J. A. Biomaterials for Tissue Engineering Applications: A Review of Past and Future Trends; Springer: New York, **2011**; p 13.
68. Wang, J.; Hu, W.; Liu, Q.; Zhang, S. *Colloids Surf. B* **2011**, *85*, 241.
69. Gil, E. S.; Frankowski, D. J.; Hudson, S. M.; Spontak, R. *J. Mater. Sci. Eng. C* **2007**, *27*, 426.
70. Zund, G.; Ye, Q.; Hoerstrup, S. P.; Schoeberlein, A.; Schmid, A. C.; Grunenfelder, J.; Vogt, P.; Turina, M. *Eur. J. Cardio-Thoracic Surg.* **1999**, *15*, 519.
71. Surewicz, W. K.; Mantsch, H. H. *Biochimica. Biophysica. Acta.* **1988**, *952*, 115.